A&A 387, 1047–1056 (2002)
DOI: 10.1051/0004-6361:20020365

Astronomy & Astrophysics

The neutral gas environment of the young supernova remnant SN 1006 (G327.6+14.6)

G. M. Dubner[1,⋆], E. B. Giacani[1,*], W. M. Goss[2], A. J. Green[3], and L.-Å. Nyman[4]

[1] Instituto de Astronomía y Física del Espacio, CC 67, Suc. 28, 1428, Buenos Aires, Argentina
e-mail: gdubner, egiacani@iafe.uba.ar
[2] National Radio Astronomy Observatory, PO Box 0, Socorro, New Mexico 87801, USA
e-mail: mgoss@aoc.nrao.edu
[3] School of Physics, University of Sydney, NSW 2006, Australia
e-mail: agreen@physics.usyd.edu.au
[4] Onsala Space Observatory, Chalmers University of Technology, 439 92 Onsala, Sweden and European Southern Observatory, Casilla 19001, Santiago 19, Chile
e-mail: lnyman@eso.org

Received 24 December 2001 / Accepted 8 March 2002

Abstract. Using the Australia Telescope Compact Array, we have carried out a survey of the H I emission in the direction of the bilateral supernova remnant (*SNR*) SN 1006 (G327.6+14.6). The angular resolution of the data is $4\farcm7 \times 3\farcm0$, and the rms noise ∼39 mJy/beam (∼0.3 K). To recover structures at low spatial frequencies, single dish data have been added to the interferometric images. We have also studied the ^{12}CO emission in the transitions $J = 1$–0 and $J = 2$–1, looking for very compact clumps of molecular gas as possible sites for the acceleration of electrons and nuclei to TeV energies associated with the γ-ray source detected on the NE limb of SN 1006. These molecular gas observations produced only marginal detections. From the present observations we conclude that the distribution of the surrounding neutral gas had no strong influence in shaping this *SNR* with a bilateral appearance. Intrinsic factors may have contributed to the present morphology. The remnant of SN 1006 appears to be evolving in a smooth environment with an atomic volume density $n_0 \sim 0.3$ cm^{-3}. The existence of an H I concentration projected on the center of SN 1006 suggests an upper limit of ∼−20 km s^{-1} on the systemic velocity of the *SNR*. This limit is compatible with a distance to the *SNR* of about 1.7 kpc, in good agreement with previous estimates. An extended H I cloud with volume density ∼0.5 cm^{-3} is detected towards the NW border of SN 1006. This concentration may be responsible for the formation of the bright Balmer filaments observed in SN 1006. The absorbing column density towards SN 1006 has been estimated to be $N_{\rm H} \sim 6.8 \times 10^{20}$ cm^{-2}, in good agreement with previous suggestions based on X-ray results.

Key words. ISM: individual objects: SN 1006 – ISM: individual objects: G327.6+14.6 – ISM: supernova remnants

1. Introduction

The Galactic supernova remnant (*SNR*) SN 1006 (G327.6+14.6) is the result of a Type Ia supernova (SN) (Schaefer 1996), probably the brightest SN observed from Earth in recorded history. SN 1006 emits throughout the whole electromagnetic spectrum, from radio wavelengths to TeV γ–rays. In the radio and X–ray regimes, SN 1006 has a bilateral appearance with two symmetric, bright limbs (towards the NE and SW) and almost no emission at the sites where the axis of symmetry intersects the SN shell (to the SE and NW). In X–rays, synchrotron emission is observed from the rims, while from the interior of the *SNR* thermal X-ray emission is detected (Willingale et al. 1996; Winkler & Long 1997; Dyer et al. 2001). At optical wavelengths, SN 1006 is one of the small number of Balmer–dominated *SNR*s, with essentially no detections of the forbidden lines typically associated with *SNR*s (Fesen et al. 1985). The brightest optical filaments are located to the NW of the *SNR* where both the radio and X–ray emission are quite faint. On the southern rim of the remnant, there is a faint thin filament extending along the

Send offprint requests to: G. Dubner,
e-mail: gdubner@iafe.uba.ar
⋆ Member of the Carrera del Investigador Científico, CONICET, Argentina.

boundary of the radio shell. More diffuse Hα appears to fill much of the SE portion of the *SNR* (Winkler & Long 1997).

SN 1006 was the first Galactic *SNR* where TeV γ–rays were detected at the 5.3 σ and 7.7 σ level (Tanimori et al. 1998). The emission is localized in the northeast (NE) limb of SN 1006. High energy γ–rays detected from *SNR*s are generally considered to originate from π^0 decays induced by collisions between swept-up matter and accelerated protons in *SNR*s. However, in the case of SN 1006 the γ–rays detected towards the NE limb are thought to be Inverse Compton (IC) radiation caused by the collision of high energy electrons with low energy photons of the 2.7 K cosmic microwave background (Aharonian & Atoyan 1999; Berezhko et al. 2000; Dyer et al. 2001; Tanimori et al. 2001). An IC origin is likely since the matter density in H I outside the shock front in SN 1006 is too low to produce γ-rays from π^0 decay (predicted densities in H I are in the range $\sim$0.05 to 0.4 cm^{-3}, Willingale et al. 1996; Laming et al. 1996). It is possible to accelerate electrons and nuclei to γ–rays energies through the interaction of *SNR*s with molecular clouds (Bykov et al. 2000). The forward and reverse shocks, if accompanied by magnetohydrodynamic turbulence, can result in high-energy γ–ray radiation.

We have investigated the neutral interstellar gas around SN 1006, looking for inhomogeneities and/or anisotropies that may explain the observed characteristics. The survey in H I is part of an ongoing project to observe the environs of bilateral *SNR*s. The physical characteristics of the surrounding ISM may determine whether the origin of the peculiar bilateral morphology is caused by intrinsic factors (like biconical outflows from central compact sources), or if the *SNR* has been shaped by the interaction with dense "walls" of interstellar gas aligned parallel to the *SNR* limbs (Gaensler 1998; Giacani et al. 2000; Dubner et al. 2002). In the case of SN 1006, investigation of the properties of the surrounding ISM may give clues as to the origin of the TeV $\gamma-$radiation, localized in only one of the two symmetrical synchrotron lobes. Furthermore, the H I observations may disclose the existence of neutral gas concentrations towards the NW, which could explain the origin of the thin Balmer filaments. From H I emission observations the absorbing H I column density required to model the X-ray emission, can be directly determined.

Our H I observations represent the first high resolution, high sensitivity HI emission study of an extensive region surrounding this large *SNR* (diameter about $0\overset{\circ}{.}5$). We have also explored the surroundings of SN 1006 in the CO molecular lines. The molecular observations (in the ^{12}CO J:1–0 and J:2–1 transitions) were carried out with high angular resolution towards the NE limb and at several points along the *SNR* shell, looking for cold, compact clumps of molecular gas that could provide localized targets to accelerate electrons to very high energies.

In the next sections we describe the observations, present the images and discuss the results.

2. Observations and data reduction

2.1. HI observations

The H I interferometer observations were made with the Australia Telescope Compact Array (ATCA; Frater et al. 1992), a 6 km east-west synthesis array located near Narrabri, NSW, Australia. Over a 12 hr period on 1999 November 5, an area of approximately $2\overset{\circ}{.}4 \times 2\overset{\circ}{.}0$ was observed using the 210 m array configuration, which provides a well-distributed $u - v$ coverage. The source was surveyed as a mosaic of 19 different pointings, following a hexagonal grid. The separation between grid-points was about $16'$, which satisfies the Nyquist sampling criterion for a primary beam of $33'$ at λ 21 cm. The observations in the HI line were centered at 1421 MHz, using 1024 channels over a bandwidth of 4 MHz. The synthesized beam of the data is $4\overset{'}{.}7 \times 3\overset{'}{.}0$ with PA = $14\overset{\circ}{.}1$ and the channel separation 0.83 km s^{-1} (velocity resolution 1 km s^{-1}). Flux density and bandpass calibration were carried out using observations of PKS B1934–638, with an assumed flux density of 14.9 Jy at 1.4 GHz. Antenna gains were calibrated using observations of the source PKS B1540–828.

The data were reduced using the `MIRIAD` package (Sault et al. 1995). After flagging and calibration, the contribution from the continuum was subtracted in the $u - v$ plane (van Langevelde & Cotton 1990), and a cube was produced using natural weighting and discarding baselines longer than 1 kλ. The cube was jointly deconvolved using the maximum entropy algorithm (Sault et al. 1996), resulting in a dataset with 800 velocity planes between –250 and +400 km s^{-1} (LSR). The rms noise was determined from the flux density in the line-free channels of this final cube, resulting in 1σ level of 0.3 K per channel. The conversion between flux density in mJy beam^{-1} and brightness temperature in K for the data is 0.013 K/(mJy/beam).

To recover structures at low spatial frequencies, the same area was observed with the single-dish, 30-m radiotelescope of the IAR, located in Villa Elisa, Argentina (Arnal et al. 2000). A 1008 channel correlator was used with a total effective bandwidth of 4 MHz, centered at 1420 MHz. The velocity resolution of the single-dish data is 1 km s^{-1}, and the rms noise per channel is 0.13 K in brightness temperature. The interferometer and single-dish data were normalized to a common temperature scale and identical velocity channel interval of 0.83 km s^{-1}. Both databases were then combined in the Fourier domain using the `MIRIAD` task `IMMERGE`. The rms noise of the combined databases was calculated in line-free channels to be 0.4 K per channel.

A new image of SN 1006 was made in the radio continuum using the MOST telescope at 843 MHz. This observation, used to compare with the new H I observations, is part of a southern sky survey (Bock et al. 1999; Green 1999) and is a full 12 hr synthesis. The resolution of this

image (included in Figs. 2 and 3) is $64'' \times 43''$ and the rms noise is $\sim$2 mJy beam^{-1}.

2.2. CO observations

The CO observations were carried out on 1999 August 10 and 11 using the 15 m Swedish-ESO Submillimetre Telescope (SEST[1]) in La Silla (Chile). We used SiS receivers to simultaneosly observe the ^{12}CO $J = 1$–0 (115 GHz) and ^{12}CO $J = 2$–1 (230 GHz) lines. The signals were fed into two Acousto-Optical spectrometers: a narrow band high-resolution spectrometer with 2000 channels, bandwidth 80 MHz, channel separation 41.7 kHz (0.054 km s^{-1} at 230 GHz), and a wide band low-resolution instrument with 1440 channels, bandwidth 1000 MHz, 700 kHz channel separation (0.9 km s^{-1} at 230 GHz, and 1.8 km s^{-1} at 115 GHz). The angular resolution is $45''$ and $23''$ for the ^{12}CO $J = 1$–0 and $J = 2$–1 transitions, respectively.

The pointing of the telescope was checked once during each observing run using the AH Sco and VX Sgr SiO maser sources at 86 GHz. The pointing errors were typically $\sim 3''$. The system was calibrated at regular intervals to provide corrected antenna temperature. The beam efficiency is 0.7 and 0.5 for the $J = 1$–0 and $J = 2$–1 transitions, respectively.

A region of $5' \times 6'$ centered on the reference position $15^{\rm h}04^{\rm m}00^{\rm s}$, $-41°49'00''$ (J2000) was surveyed in the two CO lines with low and high velocity resolutions, using 195 pointings spaced by $23''$ in both spatial coordinates. The reference position was chosen to be near the TeV γ-ray source (Tanimori et al. 1998). The data were taken in position-switched mode, with an off-source position selected to be relatively free of emission. The central velocity for these observations was –25 km s^{-1}.

In addition, 21 different profiles centered around the LSR velocity of –25 km s^{-1}, were obtained at positions distributed over the shell of SN 1006 and adjacent to it (Fig. 1). Some of the spectra, including a few positions around the γ-ray source (within the box shown in Fig. 1) were also taken at high positive and negative velocities (central LSR velocities of -2000 km s^{-1}, -1000 km s^{-1}, $+1000$ km s^{-1} and $+2000$ km s^{-1}). All spectra were Hanning smoothed to improve the signal-to-noise ratio. After an average integration time of 60 s per pointing, the noise is $\sim$0.2 K for both rotational line transitions.

There is a possible detection of a broad feature in the ^{12}CO $J = 2$–1 line between $V_{\rm LSR} \sim -15$ and ~ -25 km s^{-1} at a 2σ noise level in the two points identified by stars in Fig. 1 (near (J2000) $15^{\rm h}04^{\rm m}07^{\rm s}$, $-41°53'20''$ and $15^{\rm h}04^{\rm m}00^{\rm s}$, $-41°44'30''$). Future observations are required to confirm these possible detections.

[1] The Swedish-ESO Submillimetre Telescope (SEST) is operated by the Swedish National Facility for Radio Astronomy, Onsala Space Observatory and the European Southern Observatory (ESO).

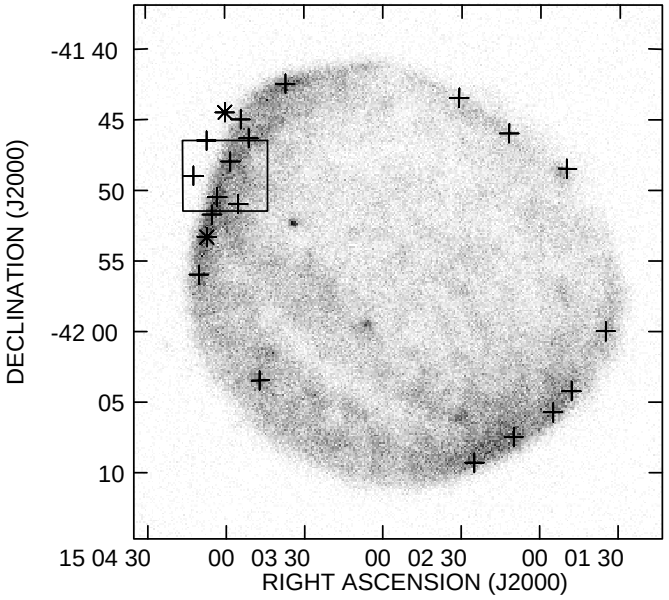

Fig. 1. *ROSAT* HRI image of SN 1006 (from Winkler & Long 1997). The box and crosses indicate the positions of the ^{12}CO $J = 1$–0 and $J = 2$–1 observations. The stars indicate the locations of possible detections.

3. Results

Figure 2 (from (a) to (d)) displays in contour lines the H I distribution within the velocity interval $(-52, +30)$ km s^{-1}, the range over which significative H I emission is detected. To produce this image we have used the interferometric data (smoothed with a $5'$ *FWHM* Gaussian) in order to easily recognize the occurrence of small scale structure. All calculations are, however, carried out using the combined (interferometric plus single dish) data. Each H I line image was obtained by averaging 5 consecutive channel images, thus spanning 4 km s^{-1}. The velocity corresponding to the first channel is shown in the top right corner of each image. These contour plots, with isophotes ranging from 2.1 K to 21 K, provide both a qualitative and quantitative image of the H I distribution in an extended field around SN 1006. The MOST image of the radio continuum emission of SN 1006 is included in greyscale in all the images for comparison.

At high negative velocities ($-52 \leq V_{\rm LSR} \leq -40$ km s^{-1}) the most conspicuous feature is the extended H I concentration located near the S–SE border of SN 1006. From $V_{\rm LSR} \sim -31$ km s^{-1} to $V_{\rm LSR} \sim -23$ km s^{-1}, the presence of an H I concentration projected onto the center of the *SNR* is quite striking. Between $V_{\rm LSR} \sim -19$ km s^{-1} and $V_{\rm LSR} \sim -11$ km s^{-1}, SN 1006 appears surrounded by smooth, tenuous gas, with a few H I concentrations scattered over the field.

At $V_{\rm LSR} \sim -6.6$ km s^{-1} an extended H I structure encompass SN 1006 along its E, N and NW sides. Within this structure, a bright H I concentration is observed towards the NW, in the direction where the brightest optical filaments are detected. This feature has two maxima centered

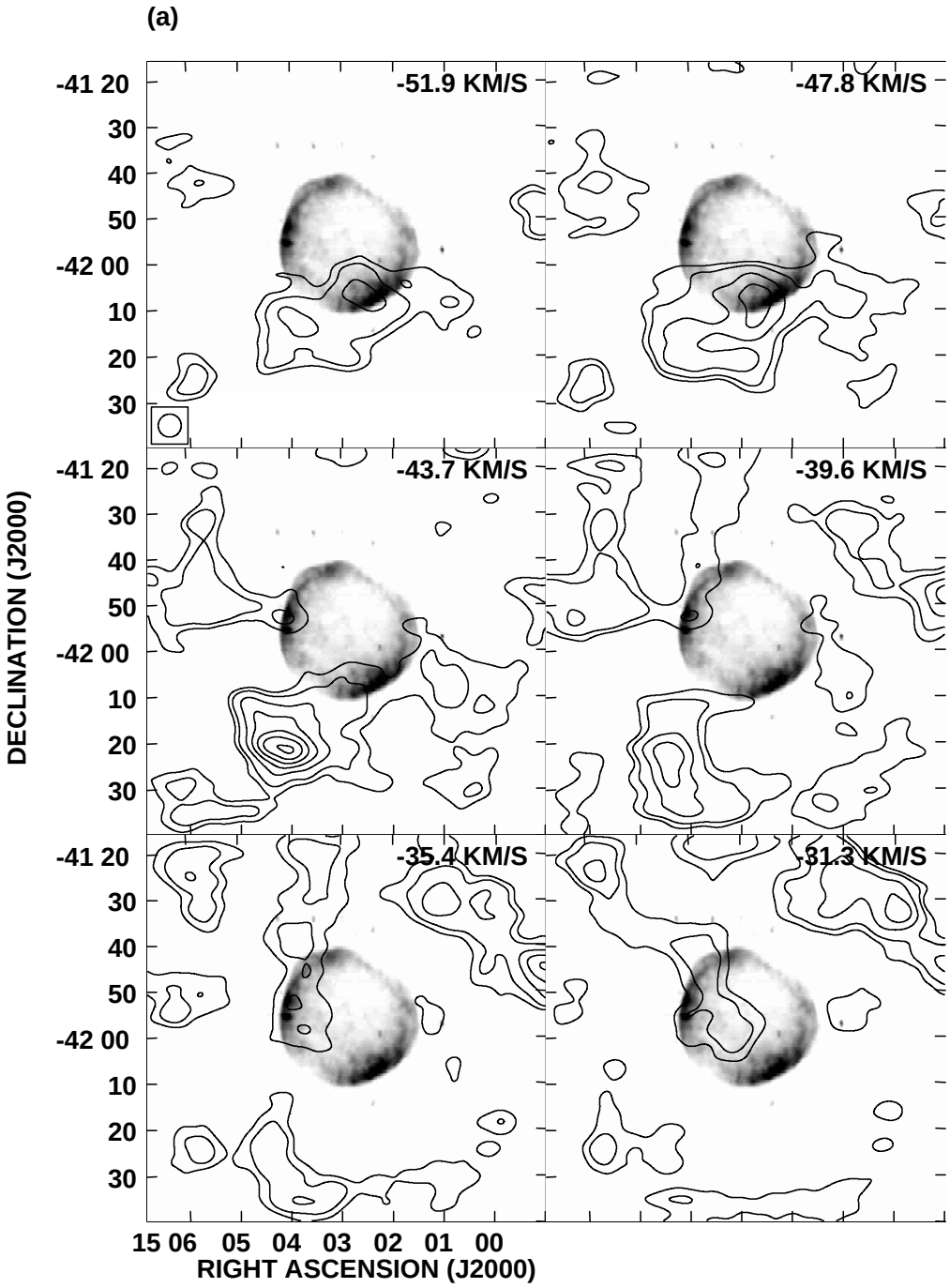

Fig. 2. From **a)** to **d)**: images of the H I data (interferometric only) between LSR velocities ~ -52 and $\sim +34$ km s^{-1}, each one integrated over 5 consecutive channels (spanning 4 km s^{-1}). The velocity shown in the upper right corner of each image corresponds to the first channel of integration. The plotted H I contours are 1.5, 2, 3, 4, 5, 6, 7, 8, 9, 12 and 15 in units of 1.4 K. The data are Gaussian smoothed to an angular resolution of $5' \times 5'$. The rms noise is 0.3 K. The MOST continuum image of SN 1006 at 843 MHz (from Bock et al. 1999) is included in greyscale for comparison.

near ($15^{\rm h}01^{\rm m}00^{\rm s}$, $-41°45'$) and ($15^{\rm h}02^{\rm m}30^{\rm s}$, $-41°35'$). Part of this feature can still be detected at $V_{\rm LSR} \sim -2.5$ km s^{-1}. At this last velocity, an H I feature delineates the E–NE border of SN 1006.

At $V_{\rm LSR} \sim +1.7$ km s^{-1}, a bright H I concentration is detected to the SW of the *SNR*, with a maximum centered near $15^{\rm h}01^{\rm m}20^{\rm s}$, $-42°10'$. The outer contour of this feature mimics the shape of the SW limb of the radio remnant. At $V_{\rm LSR} \sim +5.8$ km s^{-1}, this feature acquires an elongated NS morphology. At +5.8 km s^{-1} and at +9.9 km s^{-1}, the maximum of this feature appears adjoining the *SNR* outer border in coincidence with a small indentation of the radio continuum. At these velocities the presence of an H I concentration adjacent to the flat NW border of SN 1006, peaking near $\sim 15^{\rm h}02^{\rm m}$, $-41°40'$, is also apparent. Because this is the direction where the bright Balmer filaments are

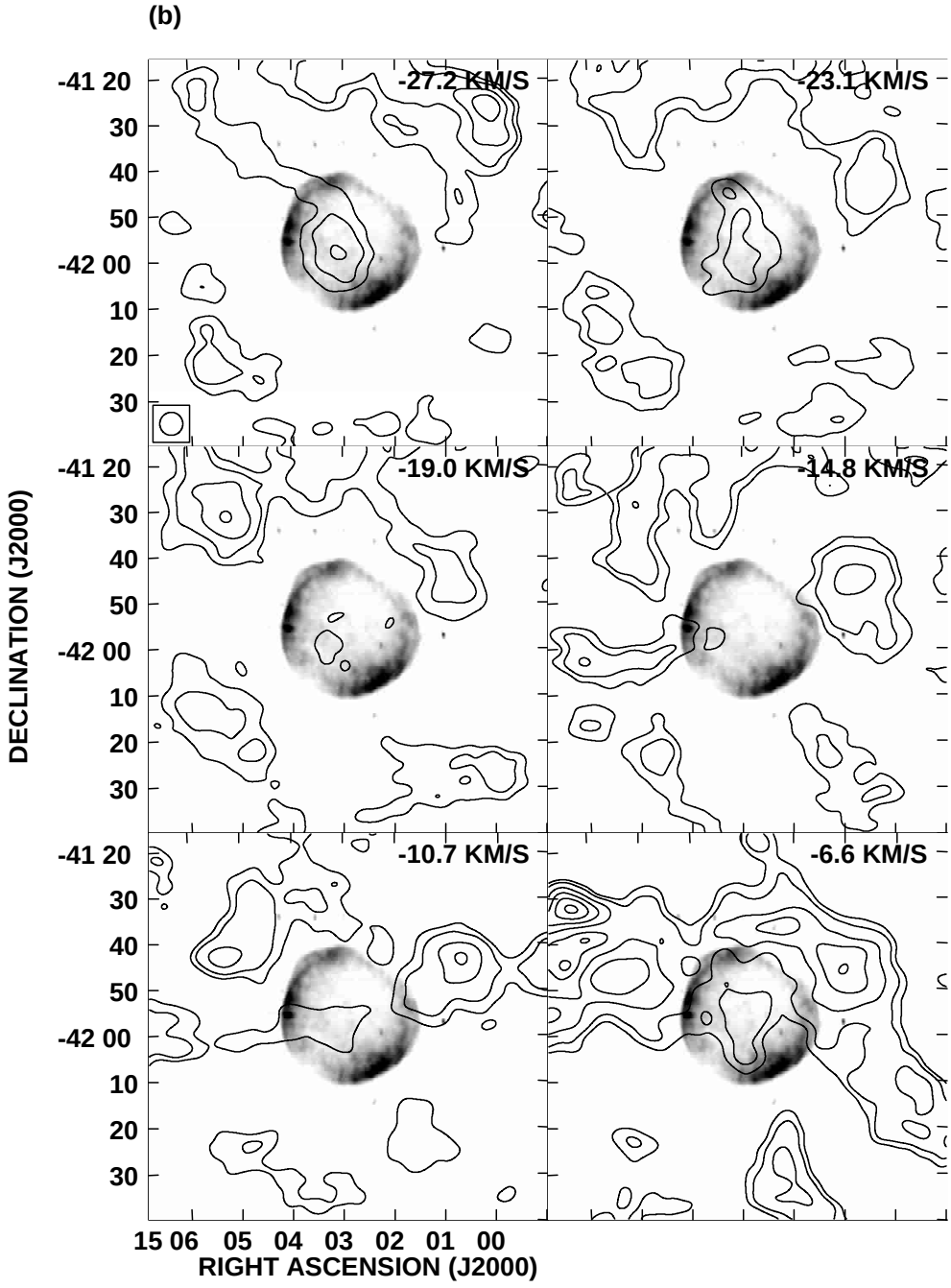

Fig. 2. continued.

detected, we will analyze this feature despite the anomalous positive velocity.

At $V_{\rm LSR} = +9.9$ km s^{-1} and $+14$ km s^{-1}, a small H I emission feature is observed projected onto the center of SN 1006. From $V_{\rm LSR} \sim +18$ km s^{-1} to $V_{\rm LSR} \sim +30$ km s^{-1}, the only noticeable feature is the concentration detected to the SE, which appears to overlap a small portion of the SE corner of SN 1006.

3.1. Analysis of the H I features

In order to understand the peculiar characteristics of SN 1006 (e.g. the bilateral appearance, the position of the brightest optical filaments, and the reason why the TeV $\gamma-$ray emission originates only on the NE lobe) it is important to estimate the preshock conditions towards different directions around SN 1006, looking for inhomogeneities and/or anisotropies in the H I distribution.

A fundamental issue in establishing a physical association between galactic H I and SN 1006 is the determination of the systemic velocity for this *SNR*. Several estimates for the distance to SN 1006 have been carried out using different methods: $d = 1.4$–2.1 kpc (Kirshner et al. 1987); $d = 0.7 \pm 0.1$ kpc (Willingale et al. 1996); $d = 1.6 \pm 0.1$ kpc (Schaefer 1996); $d = 2$ kpc (Winkler & Long 1997); $d \leq 2.1$ kpc (Burleigh et al. 2000) and

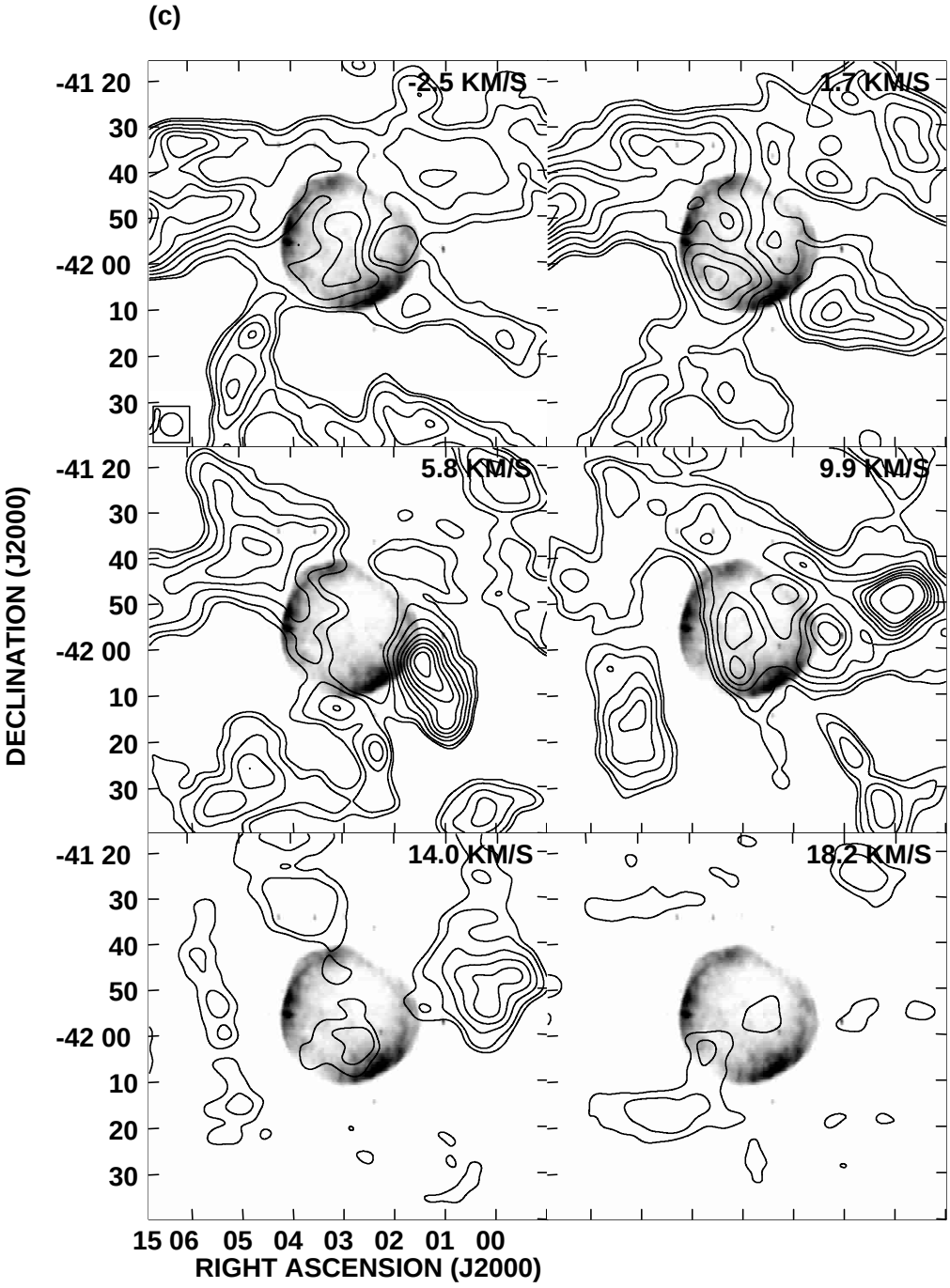

Fig. 2. continued.

d = 1.4 kpc (Allen et al. 2001). Collectively, these determinations suggest that the distance to SN 1006 lies in the range 1.4–2 kpc. The Galactic circular rotation model (Fich et al. 1989) suggests a $V_{\rm LSR}$ between $\sim$−16 and $\sim$−25 km s^{-1} for this distances range, with possible uncertainties of the order of 7 km s^{-1} because of peculiar or non-circular motions (Burton 1992). However, one must be very cautious when applying circular rotation models for sources located far from the Galactic plane, since these models are only strictly valid for low Galactic latitudes. Moreover, the warping of the Galactic plane towards negative latitudes in the fourth Galactic quadrant (Burton 1976) increases the height above the plane of an object located at a positive latitude. Here, we analyze the H I information based on morphological comparisons among the H I radiocontinuum, X-rays and optical emission from SN 1006, irrespective of the H I velocity.

As mentioned before, between $V_{\rm LSR} \sim -31$ km s^{-1} and $V_{\rm LSR} \sim -23$ km s^{-1}, an H I concentration appears projected onto the center of SN 1006. X-ray observations indicate that the interior of SN 1006 is almost free of neutral hydrogen, thus this H I feature is either in front or behind SN 1006. Based on H I observations, there is no way to accurately locate this feature along the line of sight, because

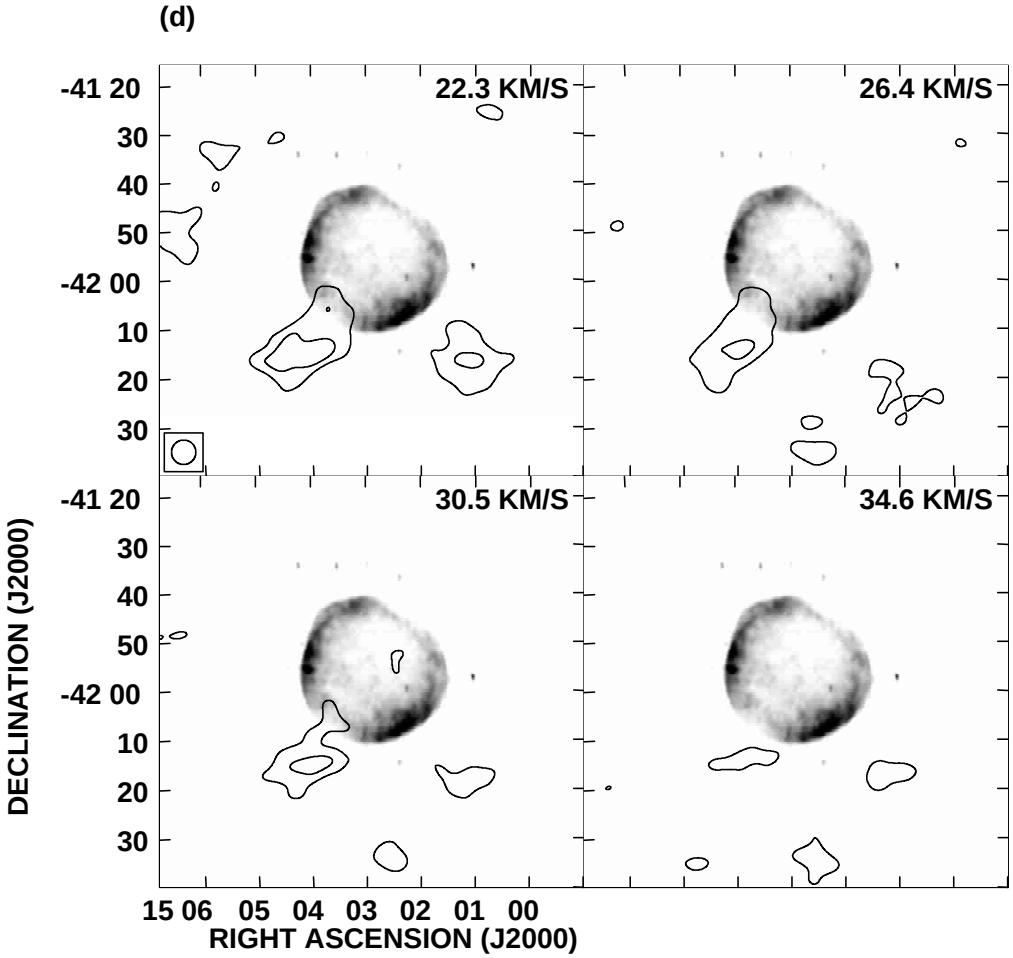

Fig. 2. continued.

the hollow center of this *SNR* precludes the use of absorption tests. If this H I cloud lies behind the *SNR*, an upper limit of $\sim$−20 km s^{-1} can be derived for the systemic velocity of SN 1006, thus suggesting an upper limit of 1.7 kpc for the distance to the remnant. Within the large uncertainties involved in the models, this limit for the distance is compatible with the average of the various distance estimates for SN 1006, as summarized above. If, on the other hand, the central H I feature would be localized in front of SN 1006, then the systemic velocity of the *SNR* would be any value more negative than $\sim$−31 km s^{-1}, more difficult to reconcile with the distance estimated for SN 1006 based on independent methods. We thus conclude that adopting $V_{\rm sys} \sim -20$ km s^{-1} and $d \sim 1.7$ kpc for the possible systemic velocity and distance to SN 1006, respectively, is a plausible hypothesis.

To investigate the average H I density in the environs of SN 1006, we have calculated the atomic density in different directions around the remnant and in each velocity plane within the interval $-20 \leq V_{\rm LSR} \leq -16$ km s^{-1}, assuming that the systemic velocity of SN 1006 lies somewhere within this range, as suggested by the present and previous results. An average density of $n_0 = 0.5$ d^{-1} cm^{-3} is obtained, where d is the distance in kpc. If $d \sim 1.7$ kpc, then $n_0 \simeq 0.3$ cm^{-3}. To carry out these calculations we have assumed that the gas is optically thin, a good approximation for gas at $b \sim +15°$, $z \sim 450$ pc. The determined value is an upper limit since contribution from unrelated distant gas with the same kinematical velocities may be included due to the distance ambiguity in this direction of the Galaxy.

The features to the north-west:

As discussed above, the flat NW border of SN 1006 is faint in radio continuum and in X-rays, but is delimited by sharp, bright optical filaments with strong Balmer lines (Long et al. 1988; Smith et al. 1991; Winkler & Long 1997). For these H_α filaments proper motions of the order of 0.30″ yr^{-1} (Long et al. 1988) and shock velocities within the range 2200–3500 km s^{-1} (Smith et al. 1991), have been estimated. Winkler & Long (1997) also detected fainter emission 2′ beyond the bright filaments to the NW.

Balmer-dominated filaments are characterized by a spectrum of Balmer lines with little or none of the characteristic forbidden-line emission of radiative filaments (such as [SII], [NII] or [OIII]). Chevalier & Raymond (1978) explained the nature of this spectrum as due to a collisionless shock moving into partially neutral interstellar material. Winkler & Long (1997) conclude that the bright optical filaments observed in SN 1006 are, in fact, thin sheets observed nearly edge-on, which originate where the shock

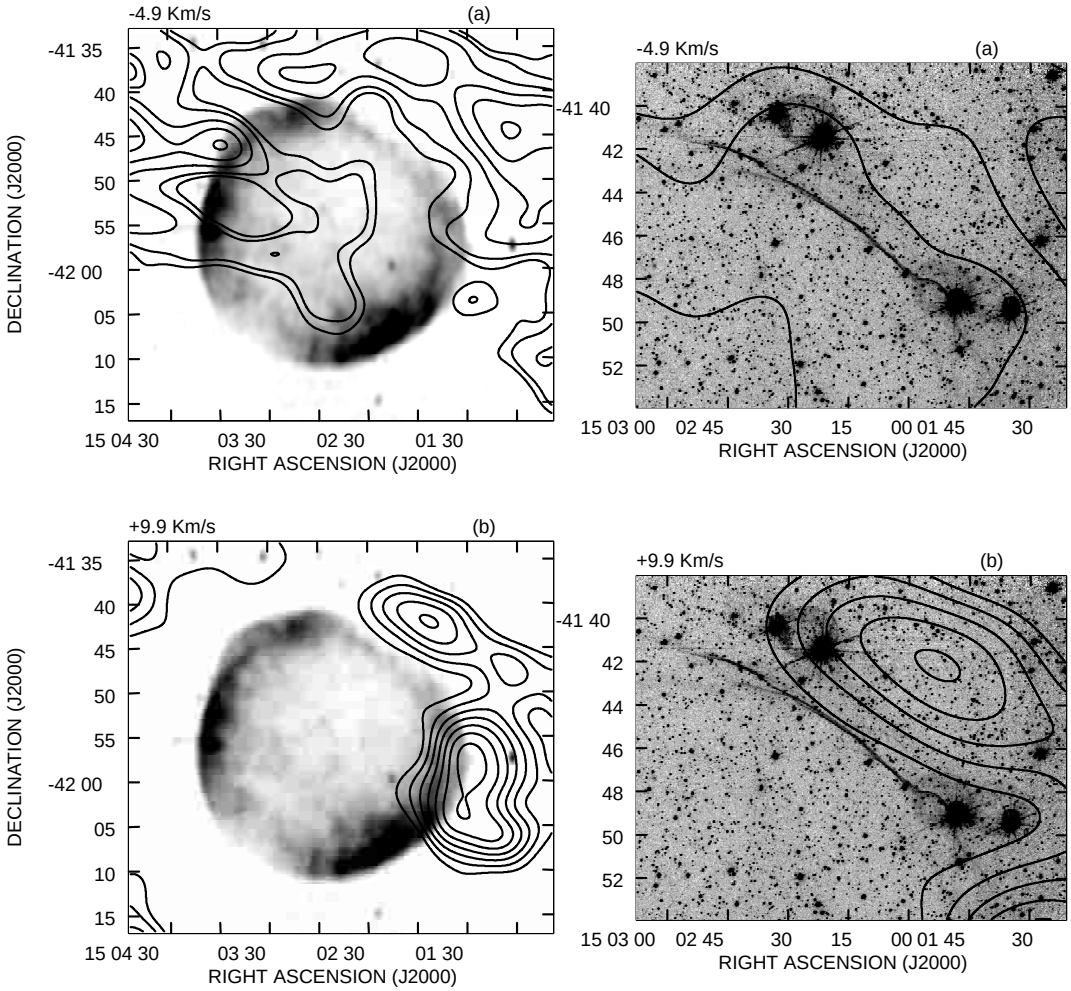

Fig. 3. a) Comparison of the H I distribution (contours) at $V_{\rm LSR} = -4.9$ km s^{-1} as obtained from the interferometric data, with the radio continuum emission of SN 1006 (from Bock et al. 1999) (left) and with the optical emission towards the NW corner of SN 1006 (from Winkler & Long 1997) (right); **b)** the same for the H I distribution at $V_{\rm LSR} = +9.9$ km s^{-1}.

encounters a "wall" with density of about 1 cm^{-3} (half of which would be ionized), oriented nearly parallel to the line of sight. The fainter filaments are formed where the SN shell encounters a lower density region. The fact that the northwest portion of SN 1006 appears flattened and expands less rapidly than elsewhere (Moffett et al. 1993; Winkler & Long 1997) is consistent with the existence of denser preshock material in this direction.

We can model a neutral "wall" with the geometry and density suggested by Winkler & Long (1997): a narrow sheet of gas with a width of 2′, comparable to the separation between bright and faint filaments (about 1 pc at the adopted distance of 1.7 kpc), a length of 15′, which is the angular size of the bright optical filaments (∼7.5 pc at $d \sim 1.7$ kpc), and a depth of 30′ along the line of sight, similar to the diameter of SN 1006 (∼15 pc at $d \sim 1.7$ kpc), with a neutral gas density of ∼0.5 cm^{-3}. This neutral hydrogen feature has a column density of $\sim 2 \times 10^{19}$ cm^{-2}, and the correspondent brightness temperature would be ∼15 K. Therefore, the present H I images should reveal the presence of the predicted feature, even taking into account the possibility that the signal may suffer from beam dilution and/or is spread over several channels.

From an inspection of the entire observed H I cube (from –250 to +400 km s^{-1}), we conclude that H I emission enhancements towards the NW occur only from $V_{\rm LSR} \sim -4.5$ km s^{-1} to $V_{\rm LSR} \sim -6.6$ km s^{-1} and from $V_{\rm LSR} \sim +9$ km s^{-1} to $V_{\rm LSR} \sim +11$ km s^{-1} (Figs. 2b and 2c). One of these two concentrations must be responsible for the particular formation of bright optical filaments exclusively on this side of the *SNR*. In Fig. 3 we display the H I distribution overlaid on the radio continuum and the optical emission (towards the NW) at these velocity ranges (Figs. 3a and 3b respectively). From the morphological point of view, the best agreement is found near +9.9 km s^{-1}, where there is an excellent correspondence between the H I and the optical emission. The major problem with this association is the discrepancy between this velocity of ∼+10 km s^{-1} and the probable systemic velocity of SN 1006 of ∼−20 km s^{-1}. Colomb & Dubner (1982) have shown the existence of two concentric expanding H I shells of swept up interstellar matter around the

SNR Lupus Loop (G330.0+15.0). Therefore, in spite of the good morphological agreement, it is possible that the observed features near +9.9 km s^{-1} are part of the slowly expanding external shell around Lupus Loop and are located at ∼300–500 pc.

On the other hand, for the NW feature observed near ∼−5 km s^{-1}, the existence of a second coincidence between the shape of the H I features and the radio continuum emission reinforces the hypothesis of association between the H I and the *SNR*. In effect, near $15^{\rm h}03^{\rm m}30^{\rm s}$, –41°45′, an H I concentration is seen apparently adjacent to SN 1006 at the position where the radio shell is broken and appears to branch off to the interior of the *SNR*. Of course, the LSR velocity of this H I concentration is still anomalous if the systemic velocity of SN 1006 is close to –20 km s^{-1}, and some kinematical perturbation has to be assumed. If there is a physical link between the NW cloud and the *SNR*, then an atomic density $n = 0.8$ d^{-1} cm^{-3} is derived ($n = 0.5$ cm^{-3} at a distance of ∼1.7 kpc). In order to calculate this density we have assumed for the elongated feature a dimension along the line of sight equal to the diameter of the *SNR*, and integrated the brightness temperature between –7 and –4 km s^{-1}. This value is in good agreement with the density proposed by Winkler & Long (1997) for the neutral component of the "wall" based on shock model fitting to the optical and X-ray data. The origin of the anomalous kinematical velocity remains an unsolved problem.

Unfortunately, there is little kinematic evidence to support the physical association of the H I with the *SNR*; projection effects and chance alignments cannot be ruled out. Thus, a quantitative analysis of the kinematical effects of this young *SNR* on the surrounding ISM, is ruled out.

3.2. The neutral hydrogen column density

In Fig. 4 we show the spatial distribution of the $N_{\rm H}$, obtained from an integration of the brightness temperature (interferometric plus single dish data) between $V_{\rm LSR} \sim -20$ km s^{-1} and $V_{\rm LSR} \sim 0$ km s^{-1}, i.e. all the H I included between the Sun and a likely systemic velocity of SN 1006. Due to the distance ambiguity in this direction of the Galaxy, gas located between ∼12 kpc and ∼14 kpc, would, in theory, contribute to the column density distribution. It is highly unlikely, however, that there is much gas located so far. Thus, the major uncertainty in considering this distribution as representative of the intervening column to the *SNR*, is the selection of the integration limit of $V_{\rm LSR} \sim -20$ km s^{-1}.

From Fig. 4 we notice that the absorbing column density decreases from the interior of SN 1006 ($N_{\rm H} \sim 7\times10^{20}$ cm^{-2}) to the radio lobes ($N_{\rm H} \sim 6.6\times10^{20}$ cm^{-2}). The maximum $N_{\rm H}$ is observed towards the NW (8×10^{20} cm^{-2}), while in the opposite direction to the SE (closer to the Galactic plane) the column density is a minimum (6×10^{20} cm^{-2}). This latter position coincides with the portion of SN 1006 with the lowest emission in all wavelengths.

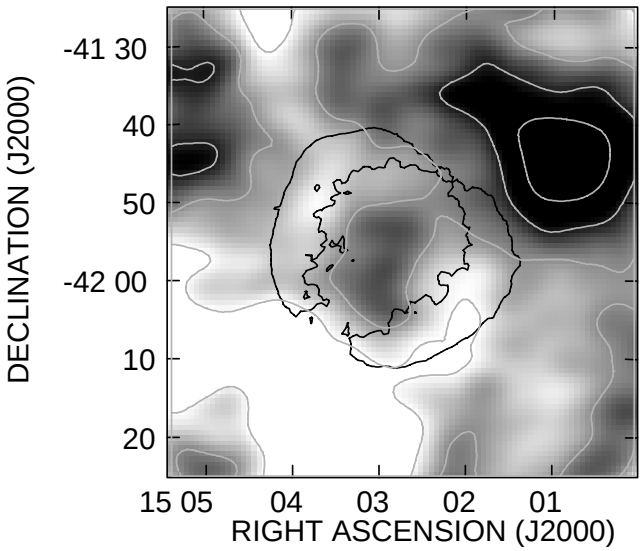

Fig. 4. H I column density integrated between 0 and −20 km s^{-1}. The greyscale varies between 6.6×10^{20} and 7.5×10^{20} cm^{-2}. The contours (in units of 10^{20} cm^{-2}) are 6.6, 7.0, 7.4 and 7.8, i.e. every three times the uncertainty in the column density estimate. The outer contour of the radio-continuum image of SN 1006 is included for reference.

4. Conclusions

We have carried out the first extensive survey of H I in a 5 square degree field around the *SNR* SN 1006 (resolution of ∼4′) in order to investigate the characteristics of the surrounding neutral interstellar medium. We have also carried out a search for cold, compact clumps of molecular gas, which may provide localized targets to accelerate electrons to TeV energies.

These new observations lead to the following conclusions: (a) The surroundings of SN 1006 are quite homogeneous, as expected at this high Galactic latitude. No obvious large-scale features are detected that can explain the *SNR* bilateral morphology based on external factors; (b) the existence of an H I concentration projected on the center of SN 1006 suggests an upper limit of ∼−20 km s^{-1} on the systemic velocity of the *SNR*. Under this assumption we obtain a limit for the distance to he *SNR* of about 1.7 kpc, in good agreement with previous estimates; (c) an average interstellar density of about 0.3 cm^{-3} is estimated for the environs of SN 1006; (d) an extensive H I concentration towards the NW, matching the location of bright Balmer filaments, is detected in the –7 to –4 km s^{-1} velocity interval. An atomic volume density of ∼0.5 cm^{-3} has been derived for this feature, in agreement with previous estimates based on optical and X-rays observations; (e) the distribution of the absorbing interstellar hydrogen between the observer and the *SNR* is quite uniform. The $N_{\rm H}$ towards SN 1006 is $\sim6.8 \times 10^{20}$ cm^{-2}, with a slight increase of the column density to the center of the *SNR*;

(f) the search for compact molecular clumps which may be the sites of acceleration of relativistic nuclei and electrons to TeV energies, produced only marginal detections at a 2σ level between $V_{\rm LSR} \sim -25$ and –15 km s^{-1}. More sensitive observations of CO and of other high excitation molecular lines are required to confirm these detections.

Acknowledgements. We thank M. Arnal for providing the HI observation from the IAR Survey for use in this paper prior to publication. We are grateful to P. F. Winkler for providing the optical image. We acknowledge the staff of ATCA for technical support during the observations. G.D., E.G., and A.J.G acknowledge the support and hospitality from NRAO during their stay at the VLA. This research was partially funded through a Cooperative Science Program between CONICET (Argentina) and the National Science Foundation (USA) and through CONICET grant 4203/96. The Australia Telescope is funded by the Commonwealth of Australia for operation as a National Facility, managed by CSIRO. The MOST is owned and operated by the University of Sydney with support from the Australian Research Council and the University of Sydney. The National Radio Astronomy Observatory is a facility of the National Science Foundation, operated under cooperative agreement by Associated Universities, Inc.

References

Aharonian, F. A., & Atoyan, A. M. 1999, A&A, 351, 330
Allen, G. E., Petre, R., & Gotthelf, E. V. 2001, ApJ, 558, 739
Arnal, M. E., Bajaja, E., Larrarte, J. J., Morras, R., & Poppel, W. G. L. 2000, A&AS, 142, 35
Berezhko, E. G., Ksenofontov, L. T., & Petukhov, S. I. 2000, in International School of Cosmic Ray Astrophysics, New Vistas in Astrophysics (Erice, Italy 1998), ed. M. M. Shapiro, R. Silberberg, T. S. Stanev, & J. P. Wefel (World Scientific Singapore), 241
Bock, D. C.-J., Large, M. I., & Sadler, E. M. 1999, AJ, 117, 1578
Burleigh, M. R., Heber, U., O'Donoghue, D., & Barstow, M. A. 2000, A&A, 356, 585
Burton, W. B. 1976, ARA&A, 14, 275
Burton, W. B., Bania, T. M., Hastmann, D., & Yuan, T. 1992, in The Galactic Interstellar Medium, ed. D. Pfeniger, & P. Bartholdi (Springer-Verlag), 1
Bykov, A. M., Chevalier, R. A., Ellison, D. C., & Uvarov, Y. A. 2000, ApJ, 538, 203
Chevalier, R. A., & Raymond, J. C. 1978, ApJ, 225, L27
Colomb, & Dubner, G. M. 1982, A&A, 112, 141
Dubner, G., Gaensler, B. M., Giacani, E., Goss, W. M., & Green, A. J. 2002, AJ, 123, 337
Dyer, K. K., Reynolds, S. P., Borkowski, K. J., Allen, G. E., & Petre, R. 2001, ApJ, 551, 439
Fesen, R. A., Blair, W. P., & Kirshner, R. P. 1985, ApJ, 292, 29
Fich, M., Blitz, L., & Stark, A. A. 1989, ApJ, 342, 272
Frater, R. H., Brooks, J. W., & Whiteoak, J. B. 1992, J. Electr. Electron. Eng. Aust., 12, 103
Gaensler, B. M. 1998, ApJ, 493, 781
Giacani, E. B., Dubner, G. M., Green, A. J., Goss, W. M., & Gaensler, B. M. 2000, AJ, 119, 281
Green, A. J. 1999, in New Perspectives on the Interstellar Medium, ed. A. R. Taylor, T. L. Landecker, & G. Joncas, ASP Conference Ser., 168, 43
Kirshner, R. P., Winkler, P. F., & Chevalier, R. A. 1987, ApJ, 315, L135
Laming, J. M. Raymond, J. C., McLaughlin, B. M., & Blair, W. P. 1996, ApJ, 472, 267
Long, K. S., Blair, W. P., & Raymond, J. C. 1988, ApJ, 333, 749
Moffett, D. A., Goss, W. M., & Reynolds, S. P. 1993, AJ, 106, 1566
Sault, R. J., Staveley-Smith, L., & Brouw, W. N. 1996, A&AS, 120, 375
Sault, R. J., Teuben, P. J., & Wright, M. C. H. 1995, in Astronomical Data Analysis Software and Systems, vol. 4, ed. R. Shaw, H. E. Payne, & J. J. E. Hayes, ASP Conf. Ser., 77, 433
Smith, R. C., Kirshner, R. P., Blair, W. P., & Winkler, P. F. 1991, ApJ, 375, 652
Schaefer, B. E. 1996, ApJ, 459, 438
Tanimori, T., Hayami, Y., Kamei, S., et al. 1998, ApJ, 497, L25
Tanimori, T. 2001, Proceedings of ICRC 2001 [astro-ph/0108031]
van Langevelde, H. J., & Cotton, W. D. 1990, A&A, 239, L5
Willingale, R., West, R. G., Pye, J. P., & Stewart, G. C. E. 1996, MNRAS, 278, 749
Winkler, P. F., & Long, K. S. 1997, ApJ, 491, 829